Innovative Food Science and Emerging Technologies 48 (2018) 42–55

Contents lists available at ScienceDirect

Innovative Food Science and Emerging Technologies

journal homepage: www.elsevier.com/locate/ifset

Radio frequency tempering uniformity investigation of frozen beef with various shapes and sizes

Yulin Li[a,b,c], Feng Li[a,b,c], Juming Tang[d], Ruyi Zhang[a,b,c], Yifen Wang[a,b,c,e], Tony Koral[f], Yang Jiao[a,b,c,*]

[a] College of Food Science and Technology, Shanghai Ocean University, Shanghai 201306, China
[b] Engineering Research Center of Food Thermal-processing Technology, Shanghai Ocean University, Shanghai 201306, China
[c] National R&D Branch Center for Freshwater Aquatic Products Processing Technology (Shanghai), Shanghai 201306, China
[d] Department of Biosystems Engineering, Washington State University, Pullman, WA 9164-6120, USA
[e] Department of Biosystems Engineering, Auburn University, Auburn, AL 36849-5417, USA
[f] Koral Associates, Woodcote, South Oxfordshire RG8 0QE, United Kingdom

ARTICLE INFO

Keywords:
Radio frequency
Tempering
Meat
Beef
Heating uniformity

ABSTRACT

Radio frequency (RF) energy generates fast and volumetric heating as it penetrates food materials and converts electromagnetic energy to heat. With these advantages, RF heating is considered as a promising technology for tempering and thawing processes in the meat and fishery products industry. However, non-uniform heating problems hinder its further application to meat products due to their various sizes and irregular shapes. This study utilized representative frozen beef samples to investigate the parameters of varying sample thickness (40 mm; 50 mm; 60 mm), base area (small:160 × 102 × 60 mm^3; medium: 220 × 140 × 60 mm^3; large: 285 × 190 × 60 mm^3) and shape (cuboid; trapezoidal prism; step) and their influence on tempering uniformity in a parallel-plate RF system. A computer simulation model was established, verified by experiments and then was utilized to evaluate the volumetric temperature distribution in food samples. Results show that the heating rate increases and heating uniformity decreases with increasing sample thickness and decreasing sample base area. As sample thickness increased from 4 cm, 5 cm to 6 cm, the simulated temperature uniformity index (*STUI*) increased from 0.093, 0.117 to 0.194. Sample base area increases from small to large decreased the *STUI* from 0.229 to 0.194 and 0.090. Among all three shapes, the cuboid shape has the best heating uniformity (*STUI* 0.194), followed by the trapezoidal prism (*STUI* 0.209) and the step shape (*STUI* 0.282). The step shape has the worst tempering uniformity because the RF energy focuses mainly on the vertical section and results in severe regional heating. Strategies to improve the step-shape frozen beef tempering uniformity by decreasing the input power to 1/3 and enlarging the electrode gap by 40 mm only reduced the hot spot temperature from 88 to 78 °C. Further research is needed in order to develop methodologies or suitable equipment for irregular shape food RF tempering in the future.

Industrial relevance: In industrial radio frequency thawing/tempering, the raw materials are usually presented in various irregular shapes and sizes. Thus, analyzing the non-uniformity severity influenced by sample size, shape and thickness to determine the capability and throughput of the equipment is necessary. Results in this study could be utilized in pre-evaluation of a protocol design and process optimization for irregular-shape food tempering.

1. Introduction

In recent decades, the amount of imported beef to China has been rising significantly to satisfy the local consumers' need of high-quality protein sources (Wu-Sheng & Cao, 2015). Before beef is exported, cows are slaughtered, cleaned, cut, and frozen to a temperature below −18 °C. After arrival, the beef parts are usually tempered for the purpose of easy cutting, either for sale or further processing. Traditional tempering processes usually allow meat products staying in a refrigeration room at 4 to 10 °C with proper air circulation. However, it typically take around 10 to 20 h to thoroughly temper large meat trunks since the natural convection heat transfer between air and frozen food material and the thermal conduction inside frozen food materials is slow (Brown & James, 2006; Uyar et al., 2015). During this lengthy

* Corresponding author at: College of Food Science and Technology, Shanghai Ocean University, Shanghai 201306, China.
E-mail address: yjiao@shou.edu.cn (Y. Jiao).

https://doi.org/10.1016/j.ifset.2018.05.008
Received 5 February 2018; Received in revised form 8 April 2018; Accepted 8 May 2018
Available online 10 May 2018
1466-8564/

tempering, the beef surfaces are exposing to relatively high temperature that would allow microbe multiplication (Manios & Skandamis, 2015; Xia, Kong, Liu, Diao, & Liu, 2012), water drip loss (Eastridge & Bowker, 2011) and meat quality deterioration. Novel fast and uniform tempering techniques are therefore needed to shorten the time and prevent food quality degradation and nutrition loss.

Radio frequency (RF) has been applied in the food industry as a novel heating technology for many years with its advantages of fast and volumetric heating characteristics. Within the 21st century, much research has been conducted on RF drying (Wang et al., 2011, 2013; Zhang, Zheng, Zhou, Huang, & Wang, 2016), tempering (Bedane, Chen, Marra, & Wang, 2017; Farag, Duggan, Morgan, Cronin, & Lyng, 2009; Llave, Terada, Fukuoka, & Sakai, 2014), sterilization (Liu, Zhang, Xu, Fang, & Zheng, 2015), and pasteurization (Gao, Tang, Villa-Rojas, Wang, & Wang, 2011; Geveke, Kozempel, Scullen, & Brunkhorst, 2002; Li, Kou, Cheng, Zheng, & Wang, 2017; Zheng, Zhang, & Wang, 2017) etc. in food industry. The principle of RF heating is that the RF generator produces a high frequency alternating electromagnetic field, and the polar molecules and charged ions in foods are agitated in the alternating field. This high speed agitation results in frictional energy loss and heat is generated within the food matrix. Research into applying RF technology to frozen food tempering and thawing started in the middle of the 20th century. Experiments have been conducted for vegetables, meat, and aquatic products on experimental and pilot scale RF heaters (Bedane et al., 2017; Llave et al., 2014; Sanders, 1966). Researchers have found that RF tempering can save 90% of the processing time comparing with traditional methodologies, and it also preserves most of the quality attributes (Farag et al., 2009; Llave et al., 2014). These research exercises have been mostly conducted with regular-shaped (normally cuboid) samples in order to simplify those experiments. However, together with the fast heating characteristic, problems of uneven heating have been found at the edges and corners of the cuboid-shape samples processed in a parallel-plate RF equipment. In order to elevate the center temperature of the frozen products to −4 °C, the edges and corners are normally over-heated to above 10 °C or even higher, which causes severe quality degradation to final tempered products (Bedane et al., 2017; Kim et al., 2016). The reasons for edge heating or non-uniform heating of RF technology has been discussed by many researchers in various applications (Alfaifi, Tang, Rasco, Wang, & Sablani, 2016; Jiao, Tang, & Wang, 2014). The established principle is that when the food material is placed in an electromagnetic field, the electromagnetic waves tend to penetrate into food materials perpendicularly to their surfaces, and the energy carried by the wave decays as it penetrates further into the food material. Since sharp edges and corners are where many surfaces converge, the electromagnetic field intensity at these locations is higher than in the rest of the sample and causes more severe heating. Edge heating also causes thermal-runaway due to the fact that dielectric loss increases as temperature increases. Compared with regular shapes such as cuboids and cylinders, irregular shapes usually have more curved surfaces, cavities and are of uneven thickness, which gives rise to the non-uniform heating patterns observed in RF heating experiments. Therefore, for irregular-shaped food products such as meat and aquatic products, the non-uniform heating problem needs to be analyzed systematically and quantitatively to allow safe industrial processing protocols to be established.

Computer simulation has the ability to solve coupling equations and demonstrate the 3D distribution of the desired parameters, which gives rise to considerable time and labor savings and reduces the need for excessive experimental work. COMSOL Multiphysics® has been utilized in RF heating process simulation in many published works (Alfaifi et al., 2014; Chen, Lau, Chen, Wang, & Subbiah, 2017; Erdogdu, Altin, Marra, & Bedane, 2017; Jiao et al., 2014; Marra, Lyng, Romano, & McKenna, 2007; Uyar et al., 2015; Zhu, Li, Li, & Wang, 2017). After being validated by practical experiments, the established model is able to demonstrate the volumetric distribution of temperature and electromagnetic fields in RF treated products, and analysis of the tempering uniformity can be made according to a developed temperature uniformity index (TUI) (Jiao, Shi, Tang, Li, & Wang, 2015).

The thickness, volume, position and orientation of the food sample can influence its heating behavior in the RF field, and the effects had been investigated by several researchers (Ferrari-John et al., 2016; Marra et al., 2007; Romano & Marra, 2008; Tiwari, Wang, Tang, & Birla, 2011a; Uyar, Erdogdu, & Marra, 2014; Uyar, Erdogdu, Sarghini, & Marra, 2016). However, most of these studies have focused on regular shaped products and not many of them have been verified experimentally (Alfaifi et al., 2016; Huang, Zhu, Yan, & Wang, 2015; Tiwari et al., 2011a; Uyar et al., 2016). The effect of sample sizes and shapes on RF tempering results has not been explored and validated systematically. A thorough understanding of all the geometrical factors including shapes and sizes and their influence would help further design RF tempering processes and improve the uniformity of RF tempering.

The purpose of this study is to (1) build up an RF tempering computer simulation model based upon a 50-ohm RF system using the COMSOL Multiphysics® software package to simulate the tempering process of frozen beef samples with selected sizes and shapes; (2) verify the accuracy of the simulation model by pilot-scale RF tempering experiments; (3) apply the model to analyze the heating uniformity index of various beef samples, and (4) explore the effect of varying the electrode gap and the RF power input in order to improve heating uniformity with a representative-shaped food sample.

2. Materials and methods

2.1. Frozen food sample preparation

A quantity of fresh lean beef was purchased from a local grocery store in Lingang, Shanghai, China. The beef samples were minced with an automatic mincer (JR-12 800W, Shangxichu, Guangzhou) and then homogenized by hand mixing before filling into cuboid polypropylene containers. The size and specific dimensions of the samples are shown in Fig. 1. Specifically, (a) (b) (c) are frozen beef samples with the same base surface area but of three different thicknesses: (a) 40 mm; (b) 50 mm; (c) 60 mm. (d) (c) (e) are samples with the same height but different base surface areas: (d) small $160 \times 102\,\text{mm}^2$; (c) medium $220 \times 140\,\text{mm}^2$; (e) large $285 \times 190\,\text{mm}^2$. (c) (f) (g) are samples with different shapes: (c) is cuboid, (f) is a trapezoidal prism shape with a corner (1/8 volume) cut off from (c), and (g) is a step shape with a corner (1/4 volume) cut from (c). It needs to be mentioned here that sample (c) was depicted three times in Fig. 1 as control since it represents “60-mm thickness”, “medium base area” and “cuboid shape” in each category, respectively.

To prepare samples (a) to (e), the minced beef was filled into containers, pressed to avoid air cavities inside samples, and then scraped flat. To prepare samples (f) and (g), clay material was firstly softened and modeled to the shape of the missing portion of the beef samples. When the clay had cooled down, it was put into the container bottoms, and then the minced beef was filled into each container to a controlled thickness and scraped flat. All beef samples with clay and containers together were placed in a freezer (BCD-610 W, SIMENS, Germany) at −30 °C for at least 24 h until the center location reached −30 °C. After freezing, the clay and frozen beef were removed from the containers and separated manually.

2.2. Computer simulation

2.2.1. Physical model

A 3D computer model was built for the test set-up, a 12 kW, 27.12 MHz, 50-ohm RF system (Labotron 12, Sairem, France). To simplify the modeling process, only the RF heating cavity and the food sample were considered in the computation process. The RF wave generation and transmission process was simplified to a voltage value assigned to the top electrode as the energy source. The system layout

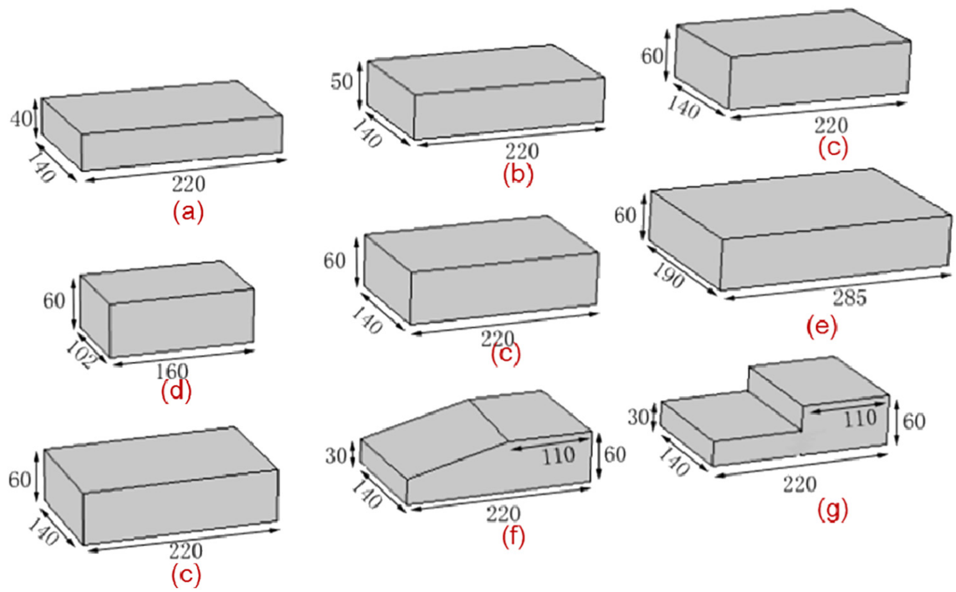

Fig. 1. The front view of frozen beef samples in selected shapes (unit: mm) (a: $220 \times 140 \times 40\,\text{mm}^3$; b: $220 \times 140 \times 50\,\text{mm}^3$; c: $220 \times 140 \times 60\,\text{mm}^3$; d: $160 \times 102 \times 60\,\text{mm}^3$; e: $285 \times 190 \times 60\,\text{mm}^3$; f: as shown; g: as shown).

and specific dimensions of the RF cavity and a frozen beef sample is shown in Fig. 2.

2.2.2. Governing equations

Maxwell's equations describe how electric and magnetic fields are generated by charges, currents, and changes of these parameters. However, solving the coupled Maxwell's equations normally requires a considerable amount of time on a high powered computer work station. Therefore, a quasi-static assumption was applied to simplify the Maxwell's equations to Laplace's equation as the governing equation in this study. This assumption has been validated by many researchers in many RF application fields to be effective (Birla, Wang, & Tang, 2008; Marra et al., 2007; Uyar et al., 2015, 2016). Laplace's equation is expressed as follows:

$$-\nabla\cdot((\sigma + j2\pi\varepsilon_0\varepsilon')\nabla V) = 0 \tag{1}$$

where σ is the electrical conductivity of the food material (S m^{-1}), $j = \sqrt{-1}$, ε_0 is the permittivity of electromagnetic wave in free space ($8.854 \times 10^{-12}\,\text{F m}^{-1}$), ε' is the dielectric constant of the food material, and V is the electric potential across the electrode gap (V). The amount of electromagnetic power converted to heat is governed by the following equation:

$$P = 2\pi f\varepsilon_0\varepsilon'' \,|\overrightarrow{E}|^2 \tag{2}$$

where P is the electromagnetic power conversion in foods per unit volume (W m^{-3}), f is the working frequency of the RF equipment (Hz), ε'' is the loss factor of the food material, and $\overrightarrow{E}$ is the electric field intensity in the food material (V m^{-1}).

When electromagnetic energy is converted to heat in food, heat transfer also occurs both inside the food volume and between the food and the atmosphere. The total heat balance during RF heating is described by the following equation:

$$\rho c_p\frac{\partial T}{\partial t} = \nabla(k\nabla T) + P \tag{3}$$

where $\partial T/\partial t$ is the instant heating rate in the food material, ($^\circ\text{C s}^{-1}$); k is the thermal conductivity ($\text{W m}^{-1}\,\text{K}^{-1}$); ρ is the density ($\text{kg m}^{-3}$); and c_p is specific heat ($\text{J kg}^{-1}\,\text{K}^{-1}$) of the food material. The heat convection between food and the atmosphere is described by the following equation:

$$Q = hA(T - T_0) \tag{4}$$

where Q is the amount of heat exchanged between the food and the atmosphere per unit time (W); h is the convective heat transfer coefficient ($\text{W m}^{-2}\,\text{K}^{-1}$); A is the surface area of the boundary between the food and the atmosphere (m^2); T is the temperature of the food surface (°C) and T_0 is the atmospheric temperature (°C).

2.2.3. Thermophysical and dielectric properties of food

Thermophysical and electrical properties of minced beef including specific heat, thermal conductivity, dielectric properties, and density which are necessary for the computer simulation were either measured or obtained from the published literature. The dielectric properties of grounded beef were measured over a temperature range of −30 to 20 °C with a vector network analyzer (Agilent PNA-L N5230C, CA, USA). The VNA was calibrated with the default calibration kit (short/50 Ω/open). A $2 \times 2 \times 2\,\text{cm}^3$ cubic sample holder was filled with the ground beef sample, and then frozen to −30 °C in a freezer (BCD-610W, SIMENS, Germany) for at least 24 h. The sample was taken out, and a hand drill was used to drill a 4 mm diameter hole from the center of the top surface to the geometrical center of the sample. The hole was to allow the insertion of a needle-probe for dielectric property measurement. The sample was returned to the freezer overnight after drilling in order to guarantee a −30 °C initial temperature. The measuring needle probe (Agilent N1501A, CA, USA), connected to the network analyzer (Agilent PNA-L N5230C, CA, USA) was inserted to the center of the sample for dielectric property measurement over a frequency range of 1 to 100 MHz. The results were converted to dielectric properties with software (85070C). A thermocouple temperature sensor (OMEGA Engineering, Norwalk, USA) was also inserted into the sample center to monitor the temperature rise. The sample, sample holder and the probe needle were put in a temperature and humidity control chamber together during measurement. Dielectric properties were measured using a temperature interval of 2 °C near to the phase transition temperature of the sample (−5 to 0 °C) and an interval of 5 °C at other temperature ranges. Triplicate measurements were taken and the average dielectric properties with standard deviations were reported at each measured temperature. The specific heat, thermal conductivity and density of lean beef at a temperature range of −18 to 10 °C were adapted from the literature (Uyar et al., 2015). Linear extrapolation was applied to the dielectric properties and thermal conductivity in the computer

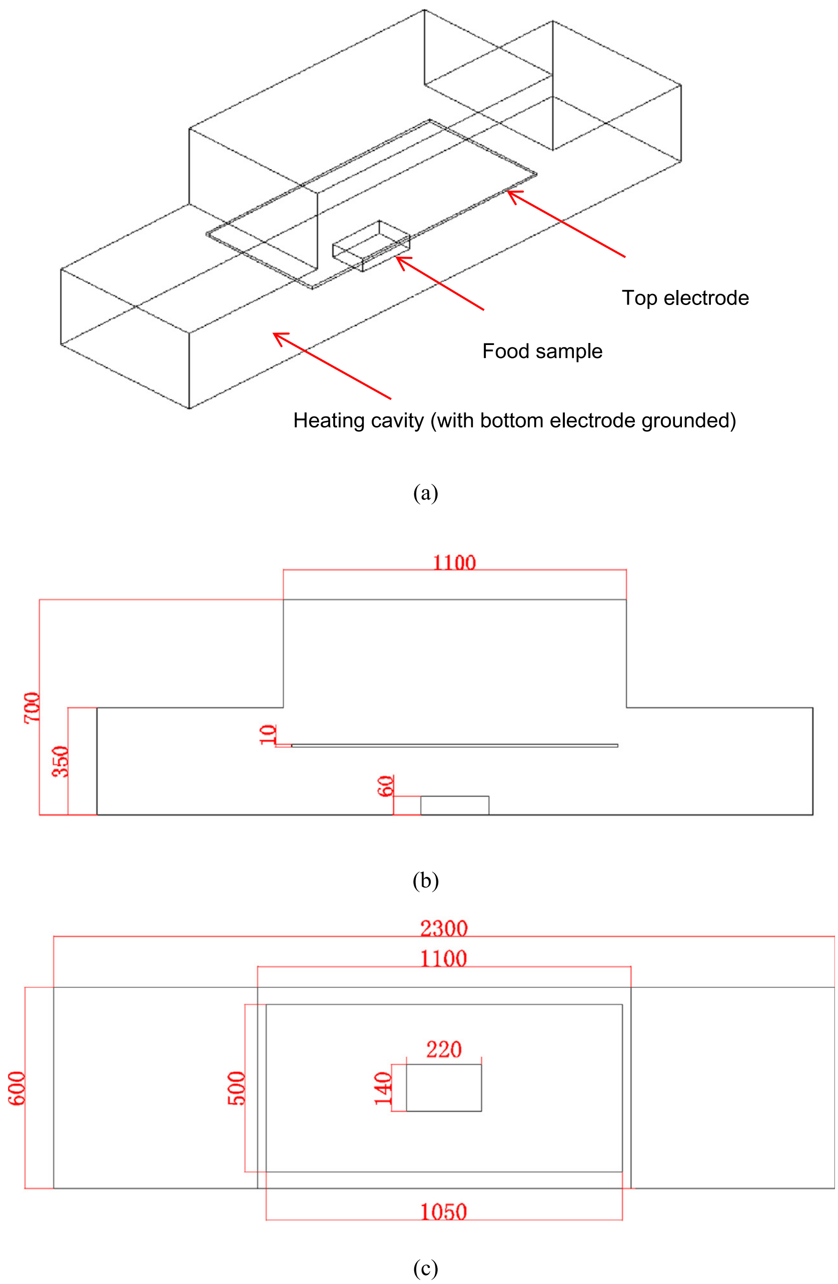

Fig. 2. Physical model of the RF cavity and food sample in RF tempering simulation including the (a) system layout, (b) front view and (c) top view with dimensions (unit: mm).

simulation for the extended temperature range.

The dielectric properties and thermal conductivity of beef samples as a function of temperature were input to the model. Since thawing was also happening in a RF tempering process due to the edge heating effect, the latent heat absorbed by the frozen product during the tempering process was taken into account as the apparent specific heat (Uyar et al., 2015). As described in the literature, constant specific heat values of the lean beef sample were assigned as 1935.2 $J\,kg^{-1}\,°C^{-1}$ at the frozen state ($T < T_{m1}$), 153,016.3 $J\,kg^{-1}\,°C^{-1}$ during the phase change ($T_{m1} \leq T \leq T_{m2}$), and 3497.4 $J\,kg^{-1}\,°C^{-1}$ at the tempered state ($T > T_{m2}$). T_{m1} and T_{m2} are defined as the initial and final temperature during the phase change process. Similarly, the density of lean beef samples also showed a constant value before, during and after phase change. Thus, constant values were assigned for each individual temperature range: 961 ($T < T_{m1}$), 1007 ($T_{m1} \leq T \leq T_{m2}$) and 1053 ($T > T_{m2}$) kg m^{-3} (Uyar et al., 2015). The phase change temperatures used in the study are $T_{m1} = -3$ °C and $T_{m2} = -1$ °C for both specific heat and density according to the reference (Farag, Lyng, Morgan, & Cronin, 2008).

These properties were assigned to the beef sample in the developed computer model (Table 1).

2.2.4. Initial and boundary conditions

The initial conditions set in the computer simulation included temperature and voltage. The initial temperature of the frozen sample was −30 °C corresponding with the experimental sample preparation. Voltage was one of the most important initial conditions as the source of electromagnetic power, and the value was obtained from experiments as shown in Table 1.

A constant temperature for the metal RF cavity and the ambient air temperature were set at 23 °C. The boundary conditions between the food sample and ambient was set as continuous. Since the food sample

Table 1
Thermophysical parameters and initial/boundary conditions used in computer simulation for RF tempering beef (*adapted from (Farag et al., 2008) and (Uyar et al., 2015)) (Tm1 = −3 °C, Tm2 = −1 °C).

Sample initial temperature	−30 [degC]			
Sample density*	$T < T_{m1}$, ρ = 961 [kg/m^3]			
	$T_{m1} \le T \le T_{m2}$, ρ = 1007 [kg/m^3]			
	$T > T_{m2}$, ρ = 1053 [kg/m^3]			
Sample specific heat*	$T < T_{m1}$, c_p = 1935.2 [J/(kg °C)]			
	$T_{m1} \le T \le T_{m2}$, c_p = 153,016.3 [J/(kg °C)]			
	$T > T_{m2}$, c_p = 3497.4 [J/(kg °C)]			
Sample dielectric properties (at 27 MHz) and thermal conductivity*	Temperature [°C]	Dielectric constant [−]	Dielectric loss factor [−]	Thermal conductivity [W/m K]*
	−30	1.2 ± 0.1	0.9 ± 0.1	1.86
	−25	1.4 ± 0.3	4.6 ± 3.2	1.71
	−18	1.5 ± 0.5	4.8 ± 2.8	1.55
	−15	19.6 ± 7.2	32.8 ± 9.6	1.43
	−10	21.3 ± 3.3	35.4 ± 8.6	1.27
	−5	39.6 ± 9.0	79.5 ± 9.1	1.19
	−3	52.3 ± 0.3	113.9 ± 5.0	0.82
	−1	69.7 ± 3.9	237.9 ± 34.7	0.57
	0	78.9 ± 1.2	241.2 ± 33.5	0.52
	1	81.8 ± 2.6	244.9 ± 38.4	0.51
	3	82.2 ± 0.5	247.0 ± 2.5	0.49
	5	83.0 ± 5.7	255.3 ± 18.3	0.47
	10	84.4 ± 5.9	290.5 ± 17.9	0.40
	15	81.6 ± 7.4	307.7 ± 35.5	0.38
	20	81.8 ± 0.3	308.3 ± 44.3	0.35
Convective heat transfer coefficient	15 [W/m^{2}K]			
Working frequency	27.12 [MHz]			
Electrode voltage	7000 to 9000 [V]			
Electrode gap	11.5 [cm]			
Surrounding temperature	20 [degC]			
Heating time	4–8 [min]			

was exposed to ambient air during RF treatment, a convective heat transfer coefficient (h) was assumed to be 15 W m^{-2} °C^{-1} for natural convection to take the heat loss into consideration. The metal enclosure of the RF cavity was set as electric insulation, which was $\nabla\cdot\overline{E} = 0$.

2.2.5. Simulation procedure

A finite element method (FEM) software COMSOL Multiphysics® (COMSOL Multiphysics 4.2, Burlington, MA, USA) was employed to simulate the RF tempering process. The joule heating module, which conjugates the electromagnetic heating with the heat transfer modules, was selected to simulate the RF tempering processes. After selecting the module, the RF heating cavity and the sample geometry were modeled in 3D with the software. Then the physical properties of the beef samples were assigned accordingly and the initial and boundary conditions were set as shown in Table 1. The meshing size for the beef samples was selected as "extra fine" and the RF cavity was meshed with a fine mesh. The mesh size was chosen based on the study of convergence when the difference of the maximum temperature between successive calculations was < 0.1%. The model was solved with the default direct solver, and the time step used in this study was 0.1 s. When the calculation was finished, the temperature distribution in the beef sample was plotted for analysis. The computation was conducted on a Dell workstation with two dual core Intel Xeon CPU 2.60 GHz processors, 128 GB RAM on a Microsoft Windows Server 2012 R2 standard operation system. The computing time used in each case varied from 25 min to 1 h for samples with various sizes and shapes. The simulation flow can be found in Fig. 3.

2.3. Tempering uniformity evaluation

After meshing the sample geometry into fine elements and solving the model, the temperature of each element was obtained to allow calculation of the *STU*I based on computer simulated temperature distribution. Tempering uniformity evaluation of all beef samples was conducted by using a simulated temperature uniformity index (*STU*I) modified from Alfaifi's work by replacing the simulated average temperature (T_{av}) with the target temperature (T_{tg}) (Alfaifi et al., 2014). Using the target temperature as a standard for evaluating the uniformity is more reasonable if one focuses on the temperature deviation from the specific required temperature. The index describes the temperature deviation of each element from the target end-point tempering temperature as expressed in Eq. (5):

$$STUI = \frac{\int |T - T_{tg}|\ dV_{vol}}{(T_{tg} - T_{initial})V_{vol}} \tag{5}$$

where T is the local temperature in the food (°C), $T_{initial}$ is the initial temperature of the food (°C), T_{tg} is the target tempering temperature, which is −4 °C in this study, and V_{vol} is the volume of the food (m^3). If more elements deviate considerably from −4 °C, the *STU*I will be higher and represents worse tempering uniformity.

2.4. RF tempering experiment

Tempering experiments were conducted on a 12 kW, 50-ohm RF heater (Labotron 12, Sairem, France). The input power was set to 3 kW with an electrode gap of 115 mm, which was selected based on preliminary experiments for a reasonable tempering rate for cuboid-shape frozen food samples.

Before conducting the RF tempering experiments, the frozen beef samples were taken out and holes (Φ2.5 mm) were drilled at specific locations for temperature monitoring purposes (Fig. 4). The temperature at sample geometrical center, corners and in-between center and corner were measured for evaluating the heating rate and validating the model for samples with various sizes and shapes. To compensate for the temperature rise due to drilling, samples were returned to the freezer overnight after drilling until the whole sample temperature reached an even −30 °C. The frozen beef samples were then taken out and placed at the center of the bottom electrode of the RF cavity for treatment. Fiber optic sensors (Heqi guangdian, Shanxi, China) were inserted into the pre-drilled holes in the samples for temperature monitoring during tempering as quickly as possible to avoid unnecessary temperature elevation of the samples. When the temperature sensors reached the

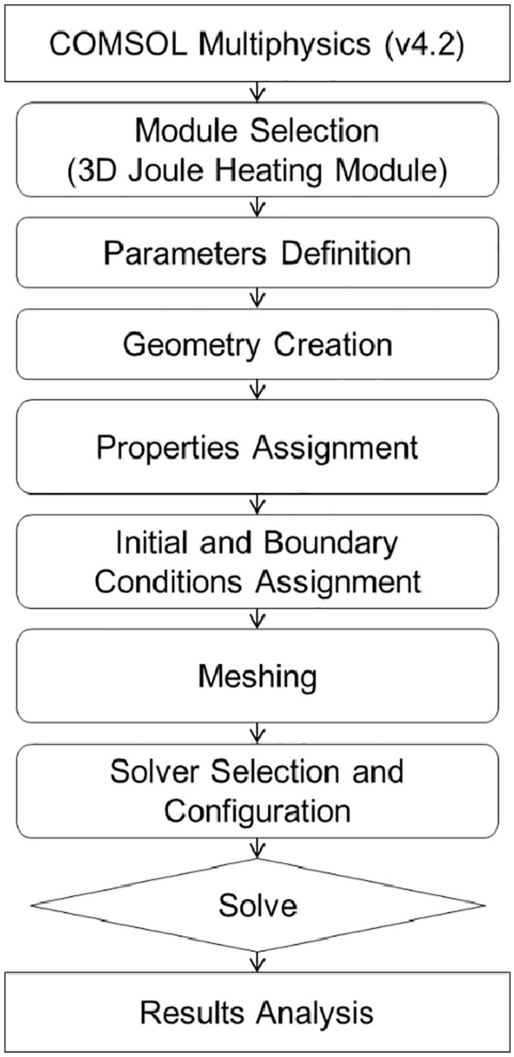

Fig. 3. Simulation procedure of a RF tempering process (modified from Jiao. et al. 2015).

sample actual temperature, the RF machine was turned on, and the data logger connected to the fiber optic sensors started to record the temperature-time history. After approximately 30 s or so for automatic circuit matching of the RF system, the temperature of the frozen beef samples started to rise. The RF machine was turned off when sensor #1 showed the sample temperature reached −4 °C, and the tempered samples were removed from the chamber as soon as possible to obtain thermal images. Thermal images of the sample surfaces from different directions (top, bottom, long and short side) were recorded by an infrared camera (A655sc, FLIR, Wilsonville, USA) for tempering uniformity evaluation and model verification. The emissivity of the camera was set as 0.95 for taking thermal images. The scheme of sample location and temperature measuring system are shown in Fig. 5. All experiments were replicated three times.

2.5. Adjusting RF treatment conditions for heating uniformity elevation

This series of RF tempering experiments were undertaken to vary the power input and electrode gap to explore how different RF power settings and electrode gaps would affect the tempering uniformity. From RF heating theory, increasing the RF power input while keeping the electrode gap constant will increase the electrode voltage (V), and this increases the electric field intensity ($\boldsymbol{E}$) in the food sample accordingly. Decreasing the electrode gap (d) while keeping the RF input power constant will also increase the electric field intensity ($\overrightarrow{E}$), and result in a higher heating rate (Eq. 6).

$$\boldsymbol{E} = V/d \tag{6}$$

As many studies have shown, increasing the electrode gap and decreasing the input power will both lower the power density in the food sample during RF heating, and result in a better heating uniformity for cuboid and sphere shaped samples (Marra et al., 2007; Romano & Marra, 2008; Tiwari, Wang, Tang, & Birla, 2011b). Here we apply the method to test its suitability for improving irregular-shaped food RF tempering uniformity. The step-shaped sample was selected since it had the worst tempering uniformity among all the shapes and sizes based upon the results from Section 2.4. Experiments were carried out to temper frozen samples using an RF power of 1, 2, and 3 kW with 115 mm electrode gap, and an RF power of 3 kW with 115, 135 and 155 mm electrode gaps, respectively. Thermal images of the long-side of the samples were taken to compare the heating uniformity after treatments with various powers and electrode gaps. The experiments were replicated twice.

2.6. Statistical analysis

Statistical analysis was conducted in order to evaluate the significance of difference between dielectric properties at different temperature range, and temperature uniformity among all shapes and sizes of samples during RF tempering. SPSS® 9.0 Software was utilized for conducting one-way ANOVA tests with $p < 0.05$.

3. Results and discussion

3.1. Dielectric properties

The dielectric properties of the beef samples at −30 to 20 °C and 27.12 MHz are reported in Table 1. Dielectric constant and loss factor showed the same increasing trend as temperature increased. Both dielectric constant and loss factor firstly increased slowly from −30 to −5 °C, and there followed a more rapid increase from −5 to 0 °C. The turning point at −5 °C was also observed for frozen tuna (Agustini, Suzuki, Hagiwara, & Ishizaki, 2001). The sudden sharp increase is due to the water molecules in foods losing their constraints during melting and becoming active in the alternating electromagnetic field. Another possible reason for the increasing loss factor is the increased amount and mobility of ions in melt water (Llave et al., 2014). Above 0 °C, the trend became flat and the temperature effect on the dielectric properties became non-significant ($p \geq 0.05$). The dielectric property data and trends in this study are comparable to those for lean beef found in the literature over the temperature range of −18 to +10 °C (Farag et al., 2008). Minor differences are possibly due to the variation in composition of the beef sample.

3.2. Tempering rate and model validation

The results in this section showed the tempering rate of the frozen beef samples with various thicknesses, base areas and shapes based on the temperature measured at the center/corner of samples (a)~(f) and the center/corner of the thick portion of samples (e) and (g). The temperatures recorded at the centers and corners of the samples were not sufficiently representative to address the RF tempering uniformity, thus the tempering uniformity is not discussed in this section. From the temperature history obtained from all the sensors, some of them showed a similar rising temperature trend. In order to better show the temperature histories to readers, only two representative locations, the center (Sensor #1) and corner temperatures (Sensor #3), were selected for plotting the time-temperature histories in Figs. 6–8.

The tempering rates of the frozen beef samples with various thicknesses under RF treatment (3 kW with 115 mm electrode gap) were

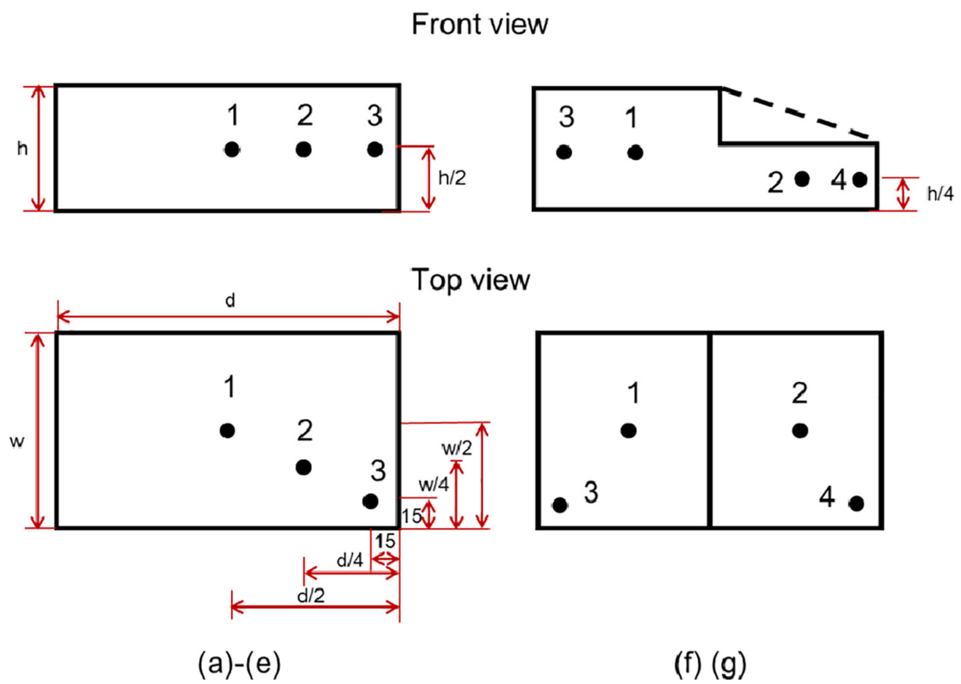

Fig. 4. Temperature sensor locations in beef samples (a)-(g) during RF tempering (unit: mm).

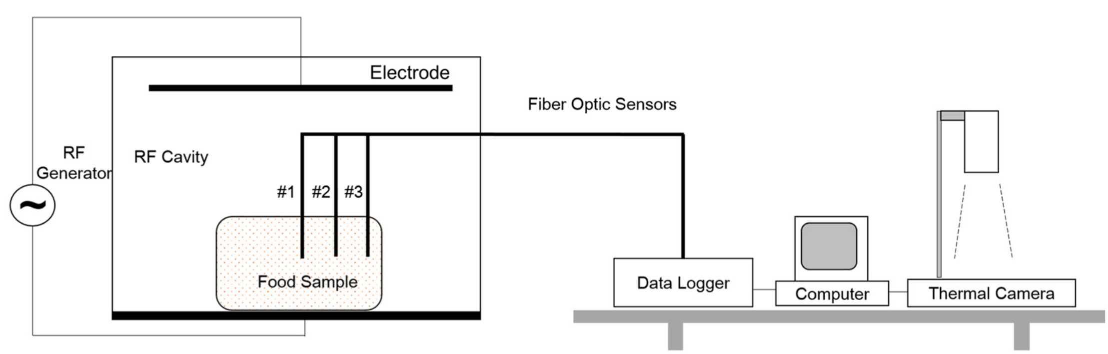

Fig. 5. Scheme of RF experimental setup including RF equipment and temperature measuring system.

compared and are shown in Fig. 6. It can be seen that the heating rate increases as the food thickness increases from 4 cm and 5 cm to 6 cm, which takes 4.8, 4.2, 3.8 min respectively to raise the temperature to −4 °C. The reason for these different heating rates is that the thicker the material is, the smaller the air gap above the material under the same electrode gap. Thus, the electric field intensity and energy

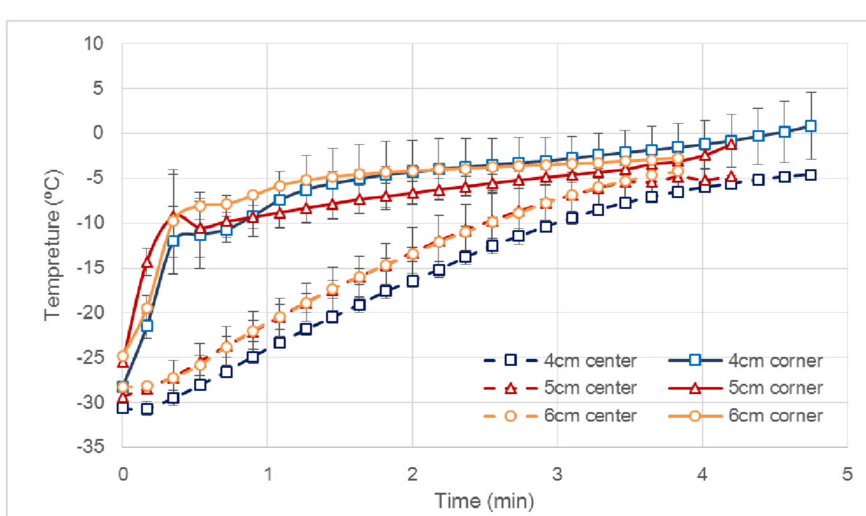

Fig. 6. Time-temperature history of cuboid-shape frozen beef with 4, 5 and 6 cm thickness during RF tempering (3 kW input power, 115 mm electrode gap).

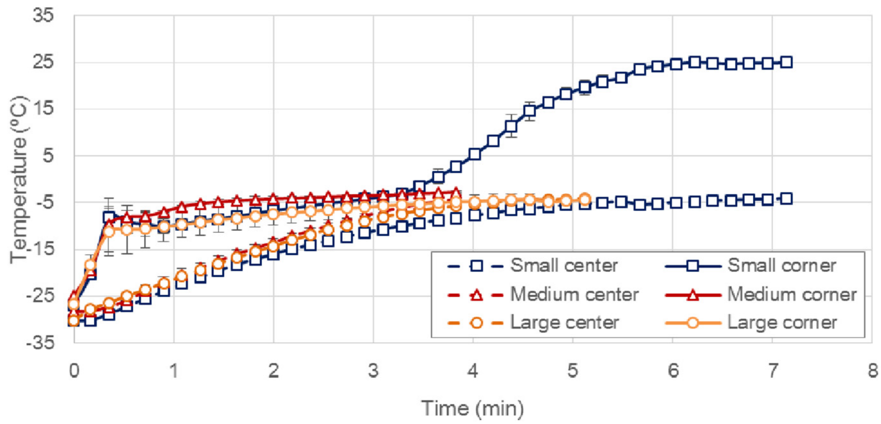

Fig. 7. Time-temperature history of cuboid-shape frozen beef with small, medium and large base area during RF tempering (3 kW input power, 115 mm electrode gap).

intensity was higher when the air gap was smaller based on electric field distribution theory.

Fig. 7 shows the tempering rate of the frozen beef in small, medium and large base area samples undergoing RF treatment using an RF input power of 3 kW and an electrode gap of 115 mm. Comparing the heating rates of three different base areas, the medium sample was tempered faster than the small and large ones. Ideally, when the same amount of input power penetrates into samples of various base areas, the electromagnetic energy increases the temperature in smaller samples faster because of its lower mass. However, due to the edge heating effect of the RF, electromagnetic energy is focused on the edges of the sample, this leads to an even more severe thermal-runaway of the heating due to the increase in the dielectric loss as the temperature increase (Jiao et al., 2014; Tiwari, Wang, Tang, & Birla, 2011c). This phenomenon is more evident for a process involving phase change. As shown in the heating curve of the small sample, the corner temperature increases suddenly to 25.0 °C after 7.1 min heating while the rest of the sample remained at under −4 °C. The thermal-runaway heating causes further energy focus on the corners and therefore the center receives insufficient energy for temperature elevation. This results in a slow heating rate at the center and a relatively longer tempering period. Medium and large samples did not show significant thermal-runaway heating. Thus, based on the mass difference, the medium base area sample was heated faster than the large one since no significant edge heating was found. It took 3.8 and 5.1 min for medium and large base area samples to reach −4 °C, respectively.

The sample shape also influences heating rates as shown in Fig. 8. Cuboid shaped samples showed a better heating uniformity since the corner and center temperature were both under −4 °C during the 3.8 min tempering process. However, both trapezoidal prisms and step shaped samples demonstrated drastic thermal-runaway heating. It was found that sample shapes with more sharp corners tended to accumulate more energy and caused serious edge/corner heating effects. Similarly for samples with various base areas, serious thermal-runaway heating was found to disturb the energy distribution for trapezoidal prisms and step shaped samples, which led to a slower heating rate at the sample center and a longer tempering period. The corner temperature was above 45 °C when the center reached −4 °C for trapezoidal prisms and step shaped samples after 5.5 and 8.6 mins RF tempering. Thus, sample shapes with more sharp corners require a slower tempering rate in the RF.

The computer simulation results and experimental results at representative locations (center (sensor #1) and corner (sensor #3)) are compared in Fig. 9 for model validation. It can be seen that while the temperatures of the whole sample volume were below 0 °C during the tempering process in the 4 cm, 5 cm, 6 cm thickness and large samples, the model provided a relatively accurate prediction (Fig. 9 (a–c)). Also, the center temperature corresponded better than the temperature at the corners from the whole heating curve. For example, there is only a deviation of 2.2 °C and 0.2 °C for corner and center for the final temperature in a 4 cm thickness sample between the experimental and simulation results (Fig. 9 (a)). Fig. 9 (b) and (c) showed that the simulated and experimental final temperatures of 5 cm and 6 cm sample differed by 2.7 and 3.5 °C at the center, and 4.1 and 5.9 °C at the corner, respectively. However, for small and trapezoidal prisms samples which showed thermal-runaway phenomena, when the temperature at some positions rose above 0 °C, the model showed larger deviations especially at the corners. As shown in Fig. 9 (d), the small samples exhibited a

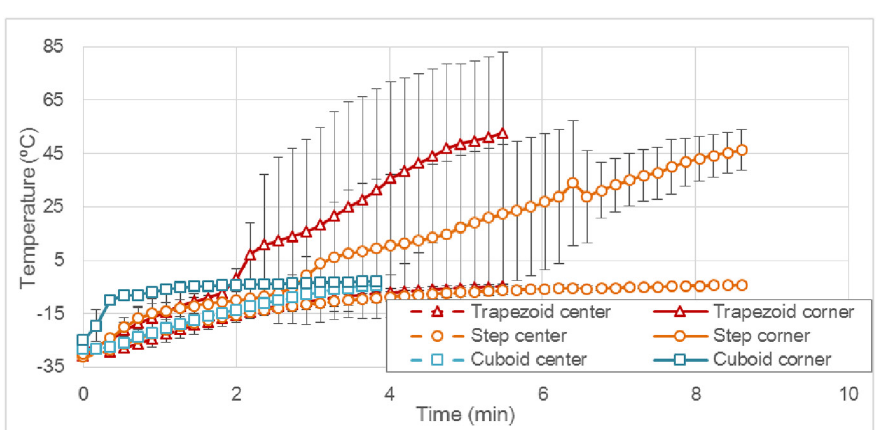

Fig. 8. Time-temperature history of frozen beef with cuboid, trapezoidal prism and step shapes during RF tempering (3 kW input power, 115 mm electrode gap).

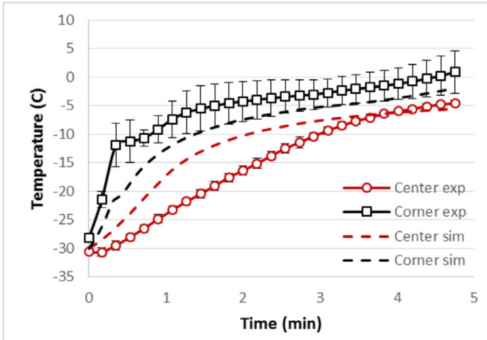

(a) 4 cm thickness

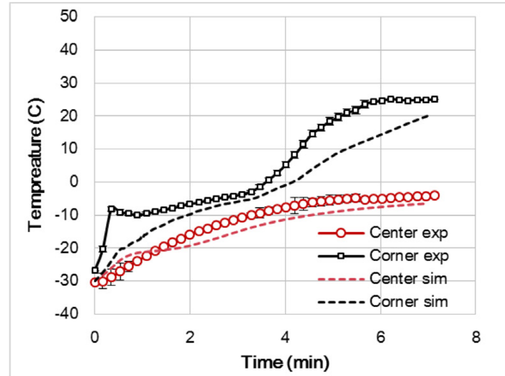

(d) Small

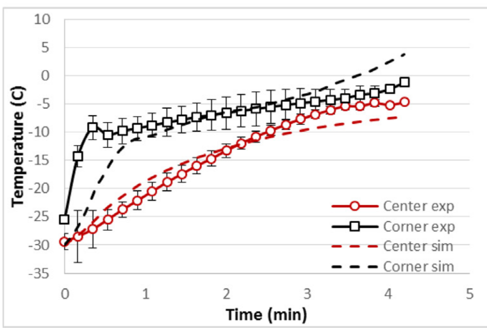

(b) 5 cm thickness

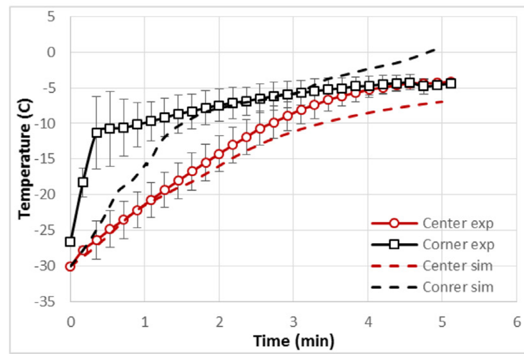

(e) Large

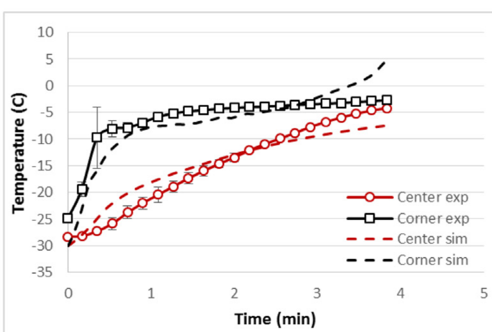

(c) 6 cm thickness / Medium Size / Cuboid Shape

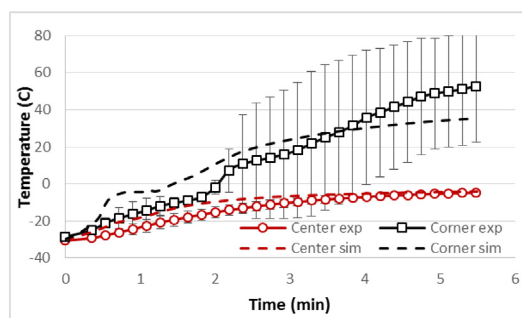

(f) Trapezoid

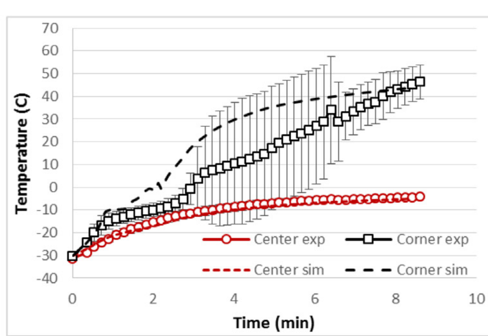

(g) Step

Fig. 9. Comparison of experimental and computer simulation results of RF tempering frozen beef with various sizes and shapes (a-g).

temperature deviation of 5.7 °C at the corners and a 0.2 °C difference at the corner. The trapezoid prism samples showed an even higher difference of 17.6 °C and the experimental final temperature is significantly higher than that obtained from the computer simulation (Fig. 9 (f)). For the step-shape sample, a relatively good agreement was observed between simulation and experiment results, the corner temperature difference is only 2.0 °C, but the trend of the heating curve of the sample corner does not follow exactly (Fig. 9 (g)). From the comparison in all cases, it could be concluded that although the edge heating could be simulated, the actual temperature and trend is different from that of the experiments in some way. This error in modeling might have been caused by accumulations of errors from different sources. During the phase transition (melting) period, a minor error due to the thermophysical and dielectric property measurement of the samples would result in a significant difference in RF power absorption, and this could have considerable effect on the predicted heating rate. Thus, inaccuracies in the food property measurements possibly exaggerates the error and finally gives rise to the huge discrepancy between the experimental and simulation results at those locations.

In order to analyze the influence of the thermophysical properties on the accuracy of the computer model, a sensitivity study was conducted based on the developed FEM model. A ± 20% variation in the dielectric properties, heat capacity, thermal conductivity and density were applied to the model, respectively, in order to obtain the final temperature for the step-shaped sample as an example. Table 2 summarizes the sensitivity analysis results and shows that the final temperatures at sample corners are sensitive to all thermophysical properties. A ± 20% change in any of the thermophysical properties will result in a temperature variation of 2 to 5 °C for sample corners. However, the center temperature was influenced insignificantly by thermophysical properties. Based on the analysis, thermophysical properties measurement accuracy could be one of the major reasons led to inaccuracy of model prediction.

3.3. Temperature distribution

The temperature distributions achieved for the frozen beef samples with various shapes, treated with the same RF input power and with the same electrode gap are shown in Fig. 10. To demonstrate the correspondence of experimental and computer simulation results, the temperature distribution of the front, top and side views of the samples after RF treatment are all shown and compared. From the side surface view, as the center temperature increases to −4 °C, the hot spot temperature at the edges and corners increases to 40.6, 46.5 and 53.4 °C for 4, 5 and 6 cm thick samples, respectively. Experimental and simulated temperature profiles from all directions showed a similar heating pattern, especially on the top and bottom surfaces, which demonstrates the effectiveness of using computer simulation as an alternative tool to reveal the temperature distribution during the RF tempering process. However, experiment results showed much more severe edge heating effect than the computer simulations for 4 cm and 5 cm thick samples, which was possibly because the computer simulation did not consider the moisture migration to the bottom and edges during tempering. This moisture migration could happen during the tempering process when the sample center reaches the target ending point. Some over-heated regions went far beyond the melting temperature. In this case, the melted water started to dissipate to areas around it or dripped/ran from the surface to the side surface and the bottom of the sample. This wet surface may result in a higher heating rate.

Table 2
Model sensitivity analysis of RF tempering final temperature of step-shape beef sample with respect to the variation of thermophysical properties.

Parameter	% change in input	Simulated final temperature (°C)	
		Center	Corner
Dielectric properties (−)	+20%	−5.4	38.7
	0	−4.9	43.7
	−20%	−3.5	49.5
Thermal conductivity (W/m K)	+20%	−5.2	37.6
	0	−4.9	43.7
	−20%	−4.8	45.6
Specific heat (J/kg K)	+20%	−6.0	39.5
	0	−4.9	43.7
	−20%	−4.3	46.3
Density (kg/m^3)	+20%	−6.0	40.4
	0	−4.9	43.7
	−20%	−4.3	47.0

Figs. 11 and 12 show the temperature distribution of frozen beef with various base areas and shapes after RF tempering, respectively. It could be seen from the samples of various base areas that the edge/corner heating is evident for samples with all base areas. The hot spot temperature was 45.7, 43.8 and 50.5 °C for small, medium and large base area samples, respectively. The relative temperature uniformity of large samples was found to be better than the medium and small ones. Uyar et al. (2016) also found that block-shaped samples with a larger base area could possibly generate better RF heating uniformity when the heating time is in a certain range. In Fig. 12, the temperature distribution varied considerably. In the trapezoidal prism samples, comparing the heating pattern at three sharp corners and two wide-angle corners using the long-side view, sharp corners had a much more intense edge heating effect. In the step-shape sample, not only the outside edges and corners were heated severely, but also the vertical portion. This is an interesting finding that normally researchers studying the regular-shape materials would only assume the outer edge as the energy focus portions (Tiwari et al., 2011a). But indeed, the electric energy focuses more on the vertical portion in a step-shape product during RF heating when both inner edge and outer edge existed, which needs further attention when developing RF heating protocols for irregular-shape products. The results showed that the trapezoidal prism shape gave a hot spot temperature of up to 74.1 °C, and the step shape resulted in an even higher hot spot temperature of 87.9 °C.

3.4. Heating uniformity evaluation

The simulated temperature uniformity index (*STUI*) was calculated for each case and is presented in Fig. 13. It can be seen from the results that the heating uniformity decreases gradually when the thickness increases from 4 cm to 5 and 6 cm since the *STUI* increases from 0.093 to 0.117 and 0.194. This is caused by the “thermal run-away” phenomena since the corner absorbs more energy than the center because of the electric field focusing effect, and the dielectric Loss factor of the beef sample increases as the temperature increases. Increasing the sample thickness reduced the air gap between the electrodes, and resulted in more power absorption. A higher heating rate normally accelerates the thermal-runaway phenomena.

When the base areas of the samples were increased, the heating uniformity increased as indicated by the *STUI* which decreases from 0.229 to 0.194 and 0.090. This is due to the fact that the severe heating zone of the sample was confined to the approximately 2 cm thick outer layer of the sample no matter what size the sample was. This phenomena has also been found by some other researchers (Alfaifi et al., 2016; Tiwari et al., 2011a). The center zone, excluding the edge heating zone, has a relatively uniform temperature distribution. Thus, as the sample base area is increased, the size of the uniformly heated zone increases much more than the non-uniformly heated zone, which results in a lower volumetric average temperature and a better heating uniformity.

The sample shape also influences the heating uniformity significantly. The cuboid and trapezoidal prism shapes had relatively similar heating uniformity, with *STUI*s of 0.194 and 0.209. This was

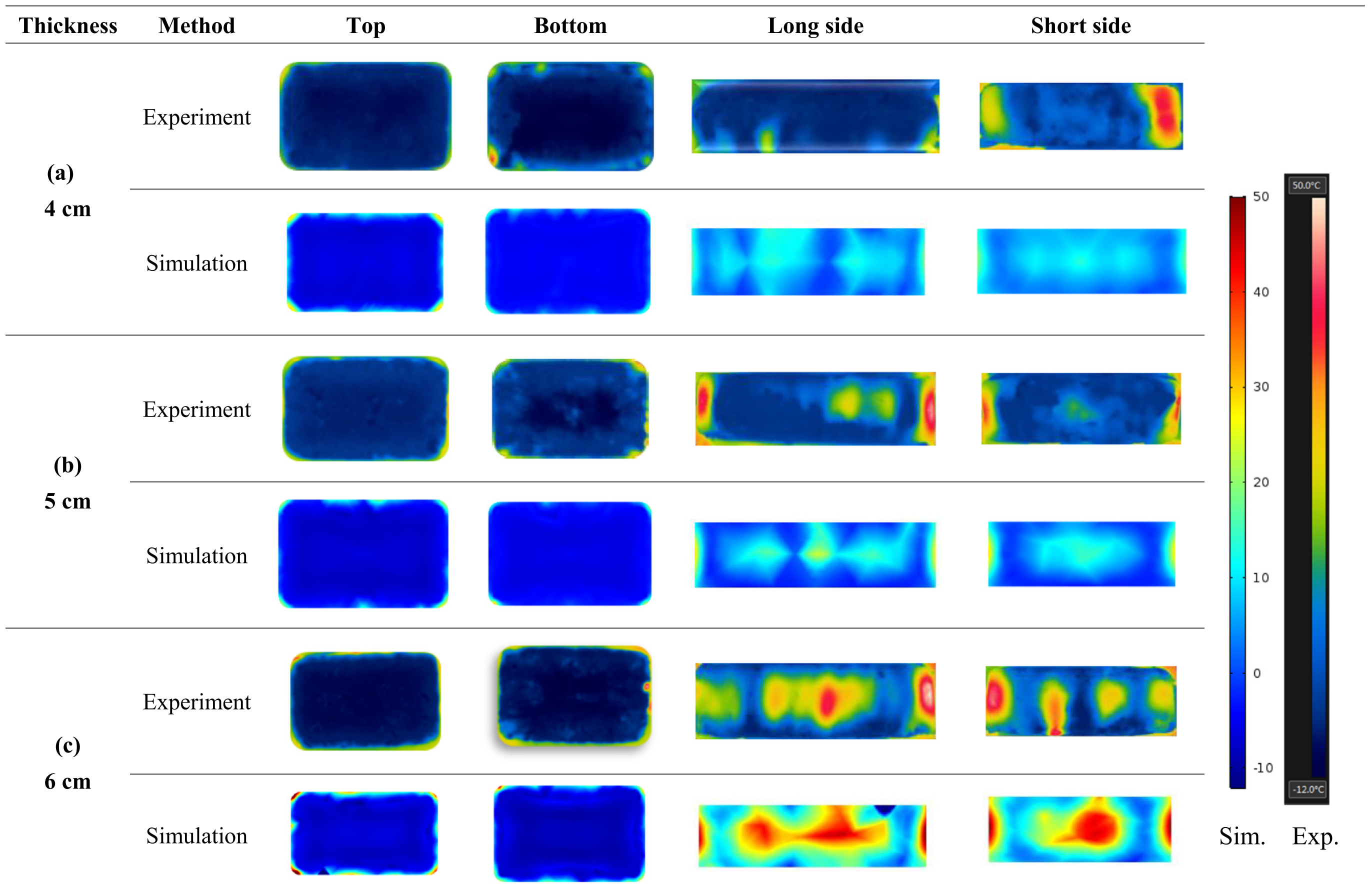

Fig. 10. Temperature distribution of frozen beef with thickness of 4, 5 and 6 cm under RF tempering treatment of 3 kW and 115 mm electrode gap with both experiment and computer simulation after 4.8, 4.2, 3.8 min treatment, respectively.

because cutting only 1/8 of the corner gave a relatively small slope, which did not have much influence on the heating uniformity. When cutting 1/4 of the corner from the cuboid shape to make it a step shape, the heating uniformity decreased significantly and the *STUI* increased to 0.282. The sharp corners caused a seriously uneven distribution of electromagnetic energy. Ferrari-John et al. (2016) found that the total number of vertices, edges and faces in the geometry and their proximity to faces perpendicular to the RF electrodes increases localized heating and decreases the uniformity. The authors also reported that positioning the sample with edges parallel to the electric field lines would result in more even temperature distribution. The findings in the current work support the results given in literature since the step-shape has more edges, vertices, faces and faces perpendicular to the electrodes than trapezoidal prism and cuboid shapes.

The *STUI* values shown in Fig. 13 correspond well with the surface temperature distribution obtained by infrared camera from Figs. 10–12. The larger the deviation of temperature on the sample surfaces, the worse heating uniformity and larger *STUI* value for the specific RF tempered samples.

3.5. Adjusting treatment conditions to elevate heating uniformity

The required tempering time and the temperature distribution of the long side view from the step shape samples are shown in Table 3. From Table 3, apparently, the tempering time increases when the RF power decreases and the electrode gap increases. When the set power was reduced from 3 kW to 2 kW and 1 kW, the tempering period increased from 5.48 to 9.17 and 14.03 min. It can be concluded generally that an RF power reduction of 1/3 would almost double the tempering period. When controlling the set power to 3 kW and changing the electrode gap from 115 mm to 135 and 155 mm, the tempering time increased from 5.48 to 7.50 and 9.33 min, respectively. Every 20 mm gap increase would increase the tempering time by 2 min. From a temperature distribution perspective, the highest power (3 kW) and smallest gap (115 mm) combination undoubtedly provides the worst heating uniformity. In this case, the highest temperature increased up to 86.9 °C. As the RF power was decreased to 1 kW, the tempering uniformity was largely improved from the color contour in Table 3. However, the hot spot temperature was 47.4 °C, which indicates unacceptable meat quality. When fixing the set power to 3 kW and increasing the electrode gap, the tempering uniformity was improved, but not as significant as with the RF power adjustment. Increasing the electrode gap to 155 mm only reduced the hot spot temperature to 71.5 °C, which was still highly deviated from the target tempering temperature. Similarly, Romano and Marra (2008) simulated cylinder, sphere and cuboid shaped food samples in RF with a power of 100 to 400 W. It was found that the lower power level used, the smaller the difference between maximum and minimum temperature. Lowering the power to 1/4 could result in a temperature difference from 18.5 to 5.5 °C for cubes and 39.32 to 24.1 °C for spheres. Thus, although varying the power and electrode gap influenced the heating uniformity, the hot spot temperatures are still too high for a tempering process. Other strategies are still needed in order to design an effective RF tempering process.

4. Conclusion

Non-uniform heating is one of the major challenges in designing RF treatments for foods. This research evaluated RF tempering effects for frozen beef samples with various thicknesses, base areas and shapes with both experimental and computer simulation methods, and

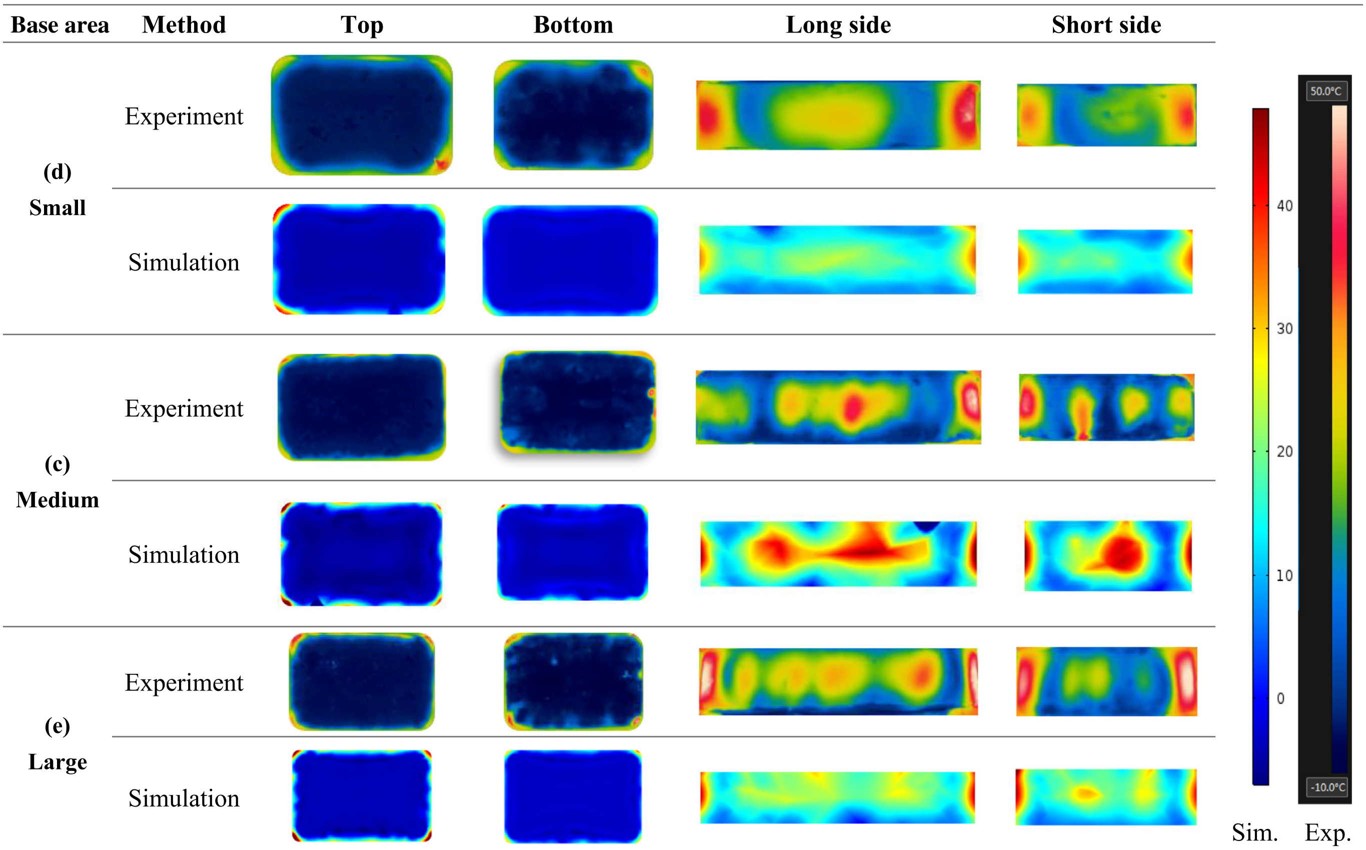

Fig. 11. Temperature distribution of frozen beef with base areas of small, medium and large under RF tempering treatment of 3 kW and 115 mm electrode gap with both experiment and computer simulation after 7.1, 5.1 and 3.8 min, respectively.

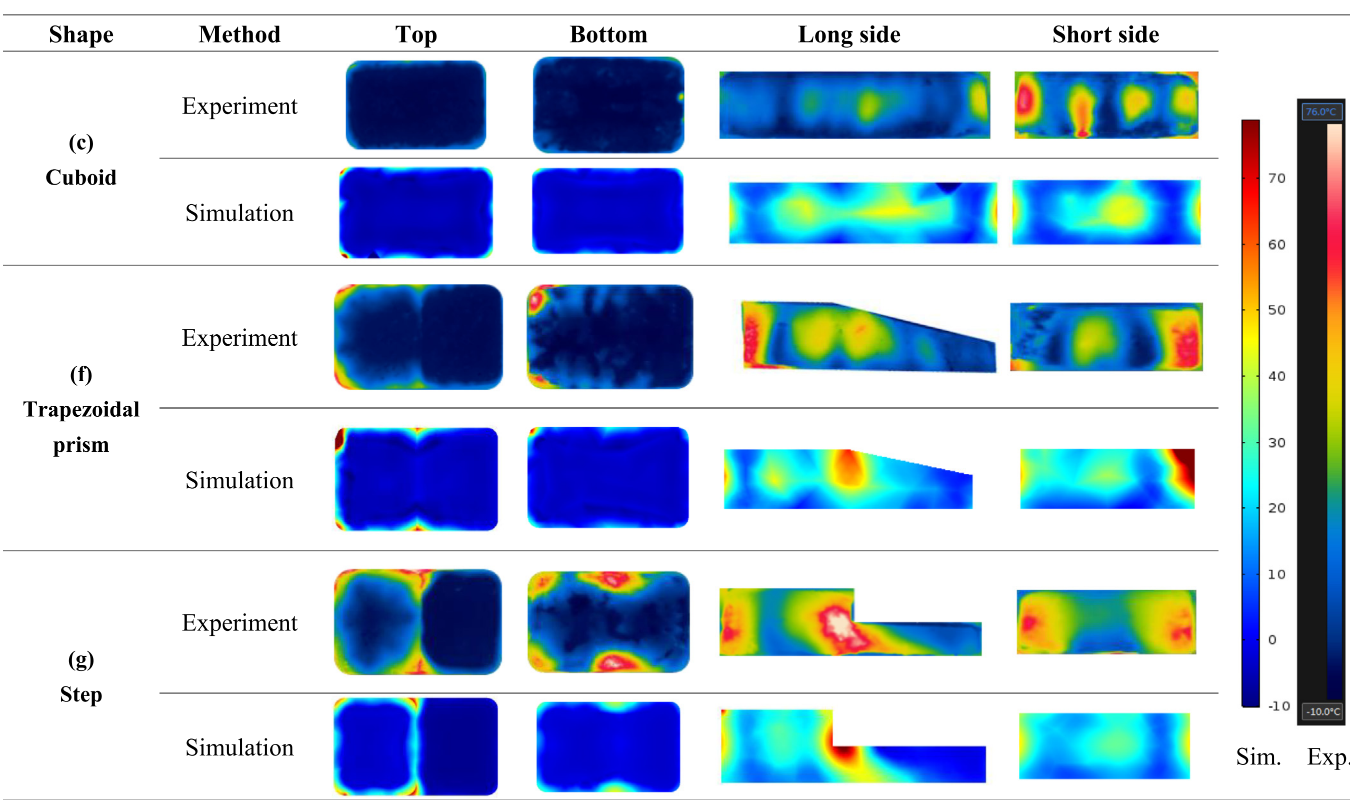

Fig. 12. Temperature distribution of frozen beef with shapes of cuboid, trapezoidal prism and step under RF tempering treatment of 3 kW and 115 mm electrode gap with both experiment and computer simulation after 8.6, 5.5 and 3.8 min, respectively.

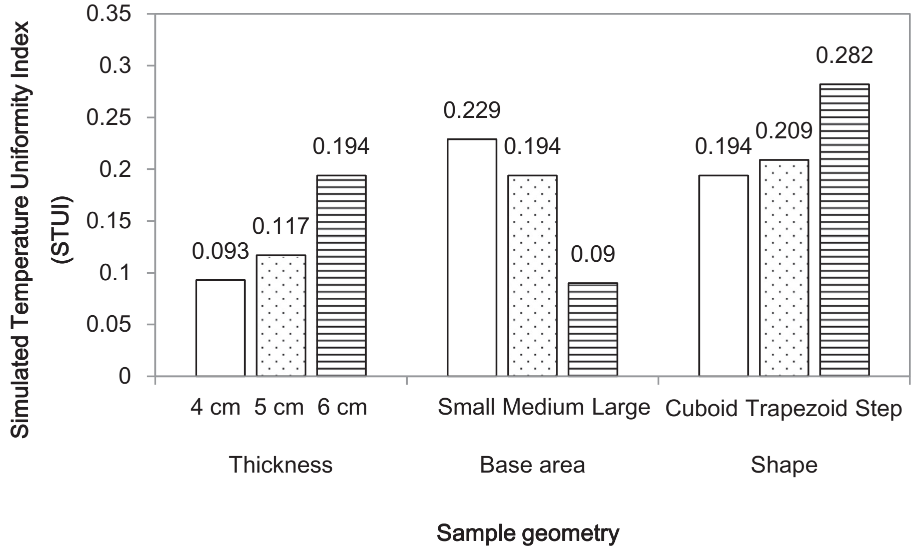

Fig. 13. Simulated temperature uniformity index (*STUI*) for RF tempered frozen beef with various thickness (a, b, c), base areas (d, c, f) and shapes (c, e, g) (denoting letters refer to Fig. 1).

Table 3
Experimental results of tempering period and temperature distribution at the side view of step-shape beef samples after RF tempering with various electrode gaps and set power (based on two replicates).

RF Treatment	1 kW 115 mm	2 kW 115 mm	3 kW 115 mm
Tempering time (min)	14.03	9.17	5.48
Temperature distribution (°C)	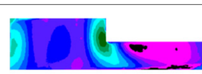	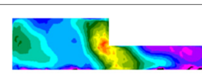	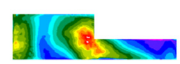
RF Treatment	**3 kW 115 mm**	**3 kW 135 mm**	**3 kW 155 mm**
Tempering time (min)	5.48	7.50	9.33
Temperature distribution (°C)	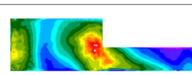	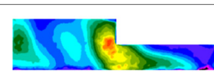	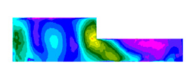

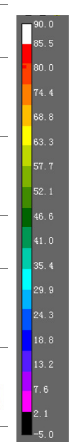

analyzed the tempering uniformity. The mathematical model generally could accurately predict the temperature distributions over the temperature range of −30 to 0 °C. However, the temperature of corners could not be accurately predicted due to the run-away heating effect. Improving the measurement accuracy of thermophysical and dielectric properties could help enhance the modeling accuracy.

Comparing the heating pattern, thicknesses, base areas and shapes of samples all greatly influenced the RF tempering uniformity. Samples with sharp edges and vertical steps tend to be the most non-uniformly heated during RF tempering. Energy focusing on the vertical section of the step-shape frozen beef sample is due to the energy focus of the multi-surface converging area. The energy focus was also along with localized energy reflection, which results in severe heating at the vertical section. Result reveals that it is necessary to avoid sharp concave facets in frozen samples during RF treatment.

Decreasing RF power and increasing electrode gap are effective in reducing the hot spot temperature at some levels, but did not lower the temperature of step-shaped samples to an acceptable level for tempering purposes. More research could be conducted on exploring the tempering uniformity of real shaped food products in RF, for example, halves or quarters of cow carcasses. Ultimately, developing fast and uniform tempering strategies for meat and aquatic products with irregular shapes will benefit the industry greatly.

Acknowledgement

The author acknowledges Shanghai Pujiang Program (16PJ1404100), Professor of Special Appointment (Youth Eastern Scholar) at Shanghai Institutions of Higher Learning (No. QD2016055), China Postdoctoral Science Foundation (2018M632299), China National Science Foundation (31571866), Shanghai Ocean University (A2-0203-00-100217 and A2-0203-00-100335) technology and development funding, and Shanghai Ocean University doctoral startup funding for their financial support to this research. The author also acknowledges Dr. Shaojin Wang from Northwest A&F University for his kindly help in manuscript revision.

References

Agustini, T. W., Suzuki, T., Hagiwara, T., & Ishizaki, S. (2001). Change of K value and water state of yellowfin tuna *Thunnus albacares* meat stored in a wide temperature range (20 °C to −84 °C). *Fisheries Science, 67*, 306–313.
Alfaifi, B., Tang, J., Jiao, Y., Wang, S., Rasco, B., Jiao, S., & Sablani, S. (2014). Radio frequency disinfestation treatments for dried fruit: Model development and validation. *Journal of Food Engineering, 120*(1), 268–276.

Alfaifi, B., Tang, J., Rasco, B., Wang, S., & Sablani, S. (2016). Computer simulation analyses to improve radio frequency (RF) heating uniformity in dried fruits for insect control. *Innovative Food Science and Emerging Technologies, 37*, 125–137.

Bedane, T. F., Chen, L., Marra, F., & Wang, S. (2017). Experimental study of radio frequency (RF) thawing of foods with movement on conveyor belt. *Journal of Food Engineering, 201*, 17–25.

Birla, S. L., Wang, S., & Tang, J. (2008). Computer simulation of radio frequency heating of model fruit immersed in water. *Journal of Food Engineering, 84*(2), 270–280.

Brown, T., & James, S. J. (2006). The effect of air temperature, velocity and visual lean (VL) composition on the tempering times of frozen boneless beef blocks. *Meat Science, 73*(4), 545–552.

Chen, J., Lau, S. K., Chen, L., Wang, S., & Subbiah, J. (2017). Modeling radio frequency heating of food moving on a conveyor belt. *Food and Bioproducts Processing, 102*, 307–319.

Eastridge, J. S., & Bowker, B. C. (2011). Effect of rapid thawing on the meat quality attributes of USDA select beef strip loin steaks. *Journal of Food Science, 76*(2), 156–162.

Erdogdu, F., Altin, O., Marra, F., & Bedane, T. F. (2017). A computational study to design process conditions in industrial radio-frequency tempering/thawing process. *Journal of Food Engineering, 213*, 99–112.

Farag, K. W., Duggan, E., Morgan, D. J., Cronin, D. A., & Lyng, J. G. (2009). A comparison of conventional and radio frequency defrosting of lean beef meats: Effects on water binding characteristics. *Meat Science, 83*(2), 278–284.

Farag, K. W., Lyng, J. G., Morgan, D. J., & Cronin, D. A. (2008). Dielectric and thermophysical properties of different beef meat blends over a temperature range of −18 to +10 °C. *Meat Science, 79*(4), 740–747.

Ferrari-John, R. S., Katrib, J., Palade, P., Batchelor, A. R., Dodds, C., & Kingman, S. W. (2016). A tool for predicting heating uniformity in industrial radio frequency processing. *Food and Bioprocess Technology, 9*(11), 1865–1873.

Gao, M., Tang, J., Villa-Rojas, R., Wang, Y., & Wang, S. (2011). Pasteurization process development for controlling Salmonella in in-shell almonds using radio frequency energy. *Journal of Food Engineering, 104*(2), 299–306.

Geveke, D. J., Kozempel, M., Scullen, O. J., & Brunkhorst, C. (2002). Radio frequency energy effects on microorganisms in foods. *Innovative Food Science & Emerging Technologies, 3*, 133–138.

Huang, Z., Zhu, H., Yan, R., & Wang, S. (2015). Simulation and prediction of radio frequency heating in dry soybeans. *Biosystems Engineering, 129*, 34–47.

Jiao, Y., Shi, H., Tang, J., Li, F., & Wang, S. (2015). Improvement of radio frequency (RF) heating uniformity on low moisture foods with Polyetherimide (PEI) blocks. *Food Research International, 74*, 106–114.

Jiao, Y., Tang, J., & Wang, S. (2014). A new strategy to improve heating uniformity of low moisture foods in radio frequency treatment for pathogen control. *Journal of Food Engineering, 141*, 128–138.

Kim, J., Park, J. W., Park, S., Dong, S. C., Choi, S. R., Yong, H. K., ... Cho, B. K. (2016). Study of radio frequency thawing for cylindrical pork sirloin. *Journal of Biosystems Engineering, 41*(2), 108–115.

Li, R., Kou, X., Cheng, T., Zheng, A., & Wang, S. (2017). Verification of radio frequency pasteurization process for in-shell almonds. *Journal of Food Engineering, 192*, 103–110.

Liu, Q., Zhang, M., Xu, B., Fang, Z., & Zheng, D. (2015). Effect of radio frequency heating on the sterilization and product quality of vacuum packaged Caixin. *Food and Bioproducts Processing, 95*, 47–54.

Llave, Y., Terada, Y., Fukuoka, M., & Sakai, N. (2014). Dielectric properties of frozen tuna and analysis of defrosting using a radio-frequency system at low frequencies. *Journal of Food Engineering, 139*, 1–9.

Manios, S. G., & Skandamis, P. N. (2015). Effect of frozen storage, different thawing methods and cooking processes on the survival of Salmonella spp. and *Escherichia coli* O157:H7 in commercially shaped beef patties. *Meat Science, 101*, 25–32.

Marra, F., Lyng, J., Romano, V., & McKenna, B. (2007). Radio-frequency heating of foodstuff: Solution and validation of a mathematical model. *Journal of Food Engineering, 79*(3), 998–1006.

Romano, V., & Marra, F. (2008). A numerical analysis of radio frequency heating of regular shaped foodstuff. *Journal of Food Engineering, 84*(3), 449–457.

Sanders, H. R. (1966). Dielectric thawing of meat and meat products. *International Journal of Food Science & Technology, 1*, 183–192.

Tiwari, G., Wang, S., Tang, J., & Birla, S. L. (2011a). Analysis of radio frequency (RF) power distribution in dry food materials. *Journal of Food Engineering, 104*(4), 548–556.

Tiwari, G., Wang, S., Tang, J., & Birla, S. L. (2011b). Analysis of radio frequency (RF) power distribution in dry food materials. *Journal of Food Engineering, 104*(4), 548–556.

Tiwari, G., Wang, S., Tang, J., & Birla, S. L. (2011c). Computer simulation model development and validation for radio frequency (RF) heating of dry food materials. *Journal of Food Engineering, 105*(1), 48–55.

Uyar, R., Bedane, T. F., Erdogdu, F., Koray Palazoglu, T., Farag, K. W., & Marra, F. (2015). Radio-frequency thawing of food products – A computational study. *Journal of Food Engineering, 146*, 163–171.

Uyar, R., Erdogdu, F., & Marra, F. (2014). Effect of load volume on power absorption and temperature evolution during radio-frequency heating of meat cubes: A computational study. *Food and Bioproducts Processing, 92*(3), 243–251.

Uyar, R., Erdogdu, F., Sarghini, F., & Marra, F. (2016). Computer simulation of radio-frequency heating applied to block-shaped foods: Analysis on the role of geometrical parameters. *Food and Bioproducts Processing, 98*, 310–319.

Wang, Y., Li, Y., Wang, S., Zhang, L., Gao, M., & Tang, J. (2011). Review of dielectric drying of foods and agricultural products. *International Journal of Agricultural & Biological Engineering, 4*(1), 1–19.

Wang, Y., Zhang, L., Johnson, J., Gao, M., Tang, J., Powers, J. R., & Wang, S. (2013). Developing hot air-assisted radio frequency drying for in-shell Macadamia nuts. *Food and Bioprocess Technology, 7*(1), 278–288.

Wu-Sheng, Y. U., & Cao, L. J. (2015). China's meat and grain imports during 2000–2012 and beyond: A comparative perspective. *Journal of Integrative Agriculture, 14*(6), 1101–1114.

Xia, X., Kong, B., Liu, J., Diao, X., & Liu, Q. (2012). Influence of different thawing methods on physicochemical changes and protein oxidation of porcine longissimus muscle. *LWT - Food Science and Technology, 46*(1), 280–286.

Zhang, B., Zheng, A., Zhou, L., Huang, Z., & Wang, S. (2016). Developing hot air-assisted radio frequency drying for in-shell walnuts. *Emirates Journal of Food and Agriculture, 28*(7), 459.

Zheng, A., Zhang, L., & Wang, S. (2017). Verification of radio frequency pasteurization treatment for controlling *Aspergillus parasiticus* on corn grains. *International Journal of Food Microbiology, 249*, 27–34.

Zhu, H., Li, D., Li, S., & Wang, S. (2017). A novel method to improve heating uniformity in mid-high moisture potato starch with radio frequency assisted treatment. *Journal of Food Engineering, 206*, 23–36.